Research Square

Preprints are preliminary reports that have not undergone peer review.
They should not be considered conclusive, used to inform clinical practice,
or referenced by the media as validated information.

Multiphase dual-energy CT parameters combined with CT features in differentiating three common lung cancers

Dongmei Liang
Gaozhou People's Hospital
Hong Zhang
Gaozhou People's Hospital
Keyu Peng
Gaozhou People's Hospital
Hongyan Ren
Gaozhou People's Hospital
Yayi Zou
Gaozhou People's Hospital
Shitao Huang
Gaozhou People's Hospital
Li'an Luo
Siemens (China)
Lveqin Huang
Siemens (China)
Hanhuan Liang
lianghanhuan@163.com

Gaozhou People's Hospital

Research Article

Keywords: Lung, Dual-energy computed tomography, Adenocarcinoma, Squamous cell carcinoma, Small cell lung cancer

Posted Date: September 25th, 2026

DOI: https://doi.org/10.21203/rs.3.rs-10793249/v1

License: This work is licensed under a Creative Commons Attribution 4.0 International License.
Read Full License

Additional Declarations: No competing interests reported.

Abstract

Objective

To evaluate the differential value of triphasic contrast-enhanced dual-energy CT (DECT) parameters combined with CT features for three common lung cancers: adenocarcinoma (AC), squamous cell carcinoma (SCC), and small cell lung cancer (SCLC).

Methods and materials

A total of 151 pathologically confirmed lung cancer patients were prospectively enrolled. Dual-source CT triphasic (arterial, venous, delayed) enhanced scans were performed to obtain DECT quantitative parameters (40/80keV CT value, spectral curve slope λHU, iodine concentration (IC), normalized iodine concentration (NIC)). Sixteen CT features were analyzed by two observers in a double-blind manner. Intraclass correlation coefficients (ICC) were used to test inter-observer consistency. Univariate/multivariate Logistic regression screened independent predictors, and DECT, CT feature, and combined models were constructed. Diagnostic efficacy was evaluated via receiver operating characteristic (ROC) curves, area under the curve (AUC), and Delong test.

Results

Among 151 patients (81 AC, 38 SCC, 32 SCLC; mean age 64.16 ± 10.25 years; 95 males, 56 females), 13 CT features and all triphasic DECT parameters showed significant differences (all $p < 0.05$). AC was predominantly peripheral (67.90%) with pleural retraction (79.01%). SCLC was mainly central (93.75%) with mediastinal lymph node fusion (87.50%). SCLC had lower parameters than AC and SCC; IC and NIC differences between AC and SCC were more prominent in venous/delayed phases. The combined model exhibited the best efficacy ($p < 0.05$ vs. single models): AUC 0.873 (AC vs. SCC), 0.980 (AC vs. SCLC), 0.937 (SCC vs. SCLC).

Conclusion

DECT parameters combined with CT features significantly improve lung cancer differentiation accuracy.

Introduction

According to the Global Cancer Statistics 2022, lung cancer ranks first among malignant tumors in both incidence and mortality rates, with its prevalence rising markedly amid population growth and aging (1, 2). Lung cancer falls into non-small cell lung cancer (NSCLC, ~ 80%–85%, including adenocarcinoma [AC] and squamous cell carcinoma [SCC]) and small cell lung cancer (SCLC, ~ 15%) (2, 3). Accurate differentiation of SCLC, SCC, and AC is pivotal to clinical treatment decision-making and prognostic

assessment, owing to pronounced differences in their biological behaviors, treatment strategies, responses, and outcomes (4–6). Thus, precise discrimination of these three histological subtypes is a critical prerequisite for reducing ineffective clinical practices, such as the indiscriminate use of chemoradiotherapy and mismatched targeted therapy.

However, non-specific early symptoms, overlapping imaging features, and biopsy sampling bias induced by tumor heterogeneity hinder precise differentiation. Quantitative parameters from Dual-energy CT (DECT) reflect tumor angiogenesis, tissue composition, and microenvironmental traits, enabling reliable tumor differentiation and overcoming the quantitative limitations of conventional CT (6–8). In oncology research, DECT's clinical value has been validated for multiple applications: benign–malignant tumor discrimination, pathological typing, lymph node assessment, invasiveness determination, gene mutation prediction, and prognostic evaluation (7, 9–12). Nevertheless, most lung cancer-focused DECT studies have key limitations, including incomplete pathological subtype coverage, single-phase scanning protocols (typically single- or dual-phase), and insufficient integration of clinical CT morphological features.

Notably, variations in DECT parameters across different contrast-enhanced phases can reveal distinct pathophysiological characteristics: differences in iodine uptake during the arterial phase correlate with tumor angiogenesis capacity, serving as a vital basis for initial subtype screening (13); DECT parameters in the venous phase stably reflect tumor parenchymal characteristics, making it the most commonly used phase for clinical subtype differentiation (4); the delayed phase focuses on contrast agent clearance kinetics within tumor tissues (14). The combined application of these three phases enables multi-dimensional complementarity, providing comprehensive functional and structural evidence to support the accurate differentiation of the three lung cancer subtypes. Therefore, this study aims to investigate the differential diagnostic value of triphasic (arterial, venous, delayed) DECT parameters combined with CT morphological features for distinguishing AC, SCC, and SCLC. We present this article in accordance with the STARD reporting checklist.

Materials and Methods

Study population

Patients with pulmonary space-occupying lesions who underwent triphasic enhanced DECT of the chest prior to treatment in our hospital from January 2022 to August 2024 were prospectively analyzed. This study was approved by the Ethics Committee of our hospital (approval number: GYLLPJ-2022049), and all patients signed informed consent forms prior to the examination.

Inclusion criteria: (1) Pathological results from surgical resection, percutaneous lung biopsy, or bronchoscopy biopsy were used as the reference standard to confirm and clarify the pathological type of lung cancer; (2) The maximum diameter of the tumor lesion was ≥ 1 cm and the lesion was solid; (3)

Complete imaging, clinical, and pathological data were available; (4) Satisfactory image quality that met the requirements for observation and data analysis.

Exclusion criteria: (1) Received any anti-tumor treatment prior to the examination; (2) Had a history of iodine contrast agent allergy; (3) Complicated with dysfunction of major organs such as the heart, liver, and kidneys.

DECT Examination

All patients underwent triphasic contrast-enhanced DECT (SOMATOM Drive, Siemens Healthineers, Forchheim, Germany) with supine positioning. Scanning range covered the whole chest; pre-injection of 30 mL normal saline (3.5 mL/s) was followed by iopromide (300 mg/mL, 1–1.2 mL/kg, 3.0 mL/s). Arterial phase was triggered 6s after aortic arch CT value reached 100 HU, venous phase at 20s delay, and delayed phase at 60s delay.

Scanning parameters: Tube voltage of A tube: 80 kV, reference tube current: 123 mAs; Tube voltage of B tube: Sn140 kV, reference tube current: 52 mAs. Pitch: 0.55, collimator width: 64×0.6 mm, matrix: 512×512, rotation time: 0.28 seconds. CARE Dose4D function was used to dynamically adjust the exposure dose. In the dual-energy scanning mode, after the completion of scanning, 80 kV and Sn140 kV images and 120 kV mixed-energy images with weighted fusion (coefficient 0.4) were automatically generated. The slice thickness and interval were 1 mm.

DECT image analysis

Two radiologists (5 + and 10 + years of experience) performed double-blind CT morphological analysis. The evaluation of CT morphological features was based on commonly used evaluation methods in previous literature (6, 15), and a total of 16 indicators (including lesion location, lobulation sign, pleural retraction, etc.) were analyzed. Consensus was reached via discussion or arbitration by a senior physician (15 + years).

The DECT images were transmitted to the post-processing workstation (Syngo.via VB20A, Siemens Healthineers, Forchheim, Germany), and the Lung PBV function and Mono+ function (Syngo.via, Dual Energy, Siemens Healthineers, Forchheim) were applied to generate target images. The DECT parameters measured included iodine concentration (IC), normalized iodine concentration (NIC), spectral curve slope (λ_{HU}), and CT value of virtual monoenergetic image (CT40/80keV). Principles for selecting the region of interest (ROI): (1) The maximum cross-section of the lesion and its adjacent two consecutive slices were selected, and each slice was measured once, totaling 3 measurements, to ensure the comprehensiveness and representativeness of the data; (2) When the lesion density was uniform, the ROI covered the maximum area of the lesion as much as possible; when the density was uneven, the area with the most solid components was selected for measurement, avoiding visually visible necrotic foci, cavitations, calcification points, vascular structures, scanning artifacts, and areas affected by

partial volume effect; (3) When measuring in different scanning phases, the ROI slice, spatial position, and size were kept consistent as much as possible; (4) All variables were measured repeatedly 3 times, and the average value was used for subsequent statistical analysis to reduce errors and improve the reliability of the results.

Statistical Analysis

Statistical analysis of data was performed using SPSS software (version 26.0; SPSS Inc., IBM Corp., IL, USA). The consistency of the measurement data between the two observers was tested using the Intraclass Correlation Coefficient (ICC). Normally distributed continuous data were expressed as mean ($\bar{x}$) ± standard deviation (s); one-way analysis of variance (ANOVA) with LSD post-hoc test was used for intergroup comparisons with homogeneous variances, while Welch's ANOVA with Tamhane T2 test was applied for heterogeneous variances. Non-normally distributed continuous data and ordinal data were presented as median (P25, P75), with Kruskal-Wallis rank sum test for three-group comparisons and Dunn's multiple comparison test for pairwise analyses. Categorical data were reported as frequency (n) and percentage (%), analyzed using chi-square test or Fisher's exact test. Parameters with intergroup statistical significance ($p < 0.05$) were included in univariate Logistic regression; eligible parameters ($p < 0.05$) were further subjected to multivariate Logistic regression (backward stepwise method) to identify independent predictors. Receiver Operating Characteristic (ROC) curves were constructed to compute the Area Under the Curve (AUC), 95% Confidence Interval (95% CI), sensitivity, and specificity. The optimal threshold was identified via Youden's index to evaluate the diagnostic efficacy of the DECT parameter model, CT morphological model, and combined model. Delong's test was used to compare AUC differences among models. All *p*-values were two-tailed, with $p < 0.05$ considered statistically significant.

Results

General Data

A total of 151 pathologically confirmed lung cancer patients were enrolled in this study, including 81 cases of AC, 38 cases of SCC, and 32 cases of SCLC (Fig. 1 and Table 1). The age of the patients ranged from 38 to 89 years, with an average of (64.16 ± 10.25) years, and there was no statistically significant difference in age distribution among the three groups ($p = 0.398$). Regarding gender composition, there were 95 males (62.91%) and 56 females (37.09%) in the overall cohort, with a significant difference in gender among the three groups ($p < 0.001$, $\chi^2 = 17.749$). Among them, SCLC had the highest proportion of males (87.50%), and AC had the highest proportion of females (51.85%). The distribution of TNM stages showed a statistically significant difference among the three groups ($p < 0.001$, $\chi^2 = 27.811$): AC was mainly in stage □ (60.49%), SCC was mainly in stage □ (52.63%), and all SCLC cases were in stages □~□ with stage □ accounting for 75.00% (Table 1). The dose-length product (DLP) of this study was (422.60 ± 125.24) mGy·cm.

Table 1
Clinical Baseline Characteristics of 151 Lung Cancer Patients

Clinical Indicators	Total (n = 151)	Adenocarcinoma (n = 81)	Squamous Cell Carcinoma (n = 38)	Small Cell Lung Cancer (n = 32)	Test Statistic (F/χ^2)	*p*-value
Age (years)					F = 0.928	0.398
- Mean ± SD	64.16 ± 10.25	64.78 ± 10.80	64.68 ± 9.23	61.97 ± 9.94		
- Range (Min ~ Max)	38 ~ 89	38 ~ 89	42 ~ 85	38 ~ 84		
Gender (n, %)					χ^2=17.749	<0.001
- Male	95 (62.91)	39 (48.15)	28 (73.68)	28 (87.50)		
- Female	56 (37.09)	42 (51.85)	10 (26.32)	4 (12.50)		
TNM Stage (n, %)					χ^2=27.811	<0.001
- Stage □	19 (12.58)	16 (19.75)	3 (7.89)	0 (0.0)		
- Stage □	5 (3.31)	3 (3.70)	2 (5.26)	0 (0.0)		
- Stage □	41 (27.15)	13 (16.05)	20 (52.63)	8 (25.0)		
- Stage □	86 (56.95)	49 (60.49)	13 (34.21)	24 (75.0)		

Notes: Age was normally distributed and expressed as "Mean ± SD" (one-way ANOVA for intergroup comparison); gender and TNM stage were categorical variables expressed as "n (%)" (Chi-square test for intergroup comparison). Staging Standard: Based on the 8th edition TNM staging system of the International Association for the Study of Lung Cancer (IASLC). Abbreviations: SD, Standard Deviation.

CT Morphological features Among Different Pathological Types of Lung Cancer

There were statistically significant differences in 13 CT morphological features among the three groups of lung cancer ($p < 0.05$), including maximum lesion diameter, location, boundary, spiculation sign, vacuole sign, calcification, vascular convergence sign, vascular involvement, pleural retraction sign, lymphadenopathy, mediastinal lymph node fusion, mediastinal structure encasement, and enhancement

characteristics; only the lobulation sign ($p = 0.165$) and cavitation sign ($p = 0.052$) showed no significant intergroup differences (Supplementary Table 1).

Thirteen CT morphological features showed significant intergroup differences ($p < 0.05$): AC was predominantly peripheral (67.90%) with high pleural retraction (79.01%) and vascular convergence sign (60.49%); SCLC was mainly central (93.75%) with mediastinal lymph node fusion (87.50%) and vascular involvement (96.88%); SCC had high obvious heterogeneous enhancement (57.89%). Lobulation sign ($p = 0.165$) and cavitation sign ($p = 0.052$) showed no significant differences. Lesion diameter: SCLC (7.14 ± 2.22 cm) > SCC (5.48 ± 1.67 cm) > AC (4.23 ± 1.52 cm) ($p < 0.001$).

DECT Parameters Among Different Pathological Types of Lung Cancer

The ICC of DECT quantitative parameter measurements in the arterial, venous, and delayed phases among the three groups of lung cancer ranged from 0.871 to 0.979. All quantitative parameters (CT40keV, CT80keV, spectral curve slope λ_{HU}, IC, NIC) showed significant differences ($p < 0.001$) (Table 2, Supplementary Table 2, and Fig. 2).

Table 2
Complete Triple-Phase Quantitative CT Parameters Among Lung Cancer Subtypes

Parameters	Phase	Adenocarcinoma (n = 81)	Squamous Cell Carcinoma (n = 38)	Small Cell Lung Cancer (n = 32)	*p*-value (Three-Group Comparison)
Virtual Monoenergetic CT Value (HU)					
CT40keV	Arterial	116.64 ± 20.95	116.56 ± 26.64	93.36 ± 17.38	< 0.001
	Venous	134.90 (123.55, 152.55)	123.40 (105.30, 147.00)	104.95 (97.33, 112.38)	< 0.001
	Delayed	142.00 (127.80, 158.20)	126.85 (112.75, 145.35)	104.40 (92.30, 119.80)	< 0.001
CT80keV	Arterial	60.07 ± 6.65	59.54 ± 8.65	53.36 ± 5.27	< 0.001
	Venous	65.40 ± 6.77	62.02 ± 7.69	55.05 ± 5.10	< 0.001
	Delayed	66.10 (62.65, 70.55)	63.20 (58.88, 67.03)	55.15 (53.05, 57.40)	< 0.001
Spectral Curve Slope					
λ_{HU} (40 ~ 80keV)	Arterial	1.41 ± 0.44	1.43 ± 0.49	1.00 ± 0.36	< 0.001
	Venous	1.78 (1.50, 2.15)	1.52 (1.21, 2.01)	1.24 (1.08, 1.46)	< 0.001
	Delayed	1.92 ± 0.42	1.64 ± 0.40	1.25 ± 0.36	< 0.001
Iodine-Related Parameters					
Iodine Concentration (IC, mg/mL)	Arterial	0.90 (0.70, 1.10)	1.00 (0.60, 1.20)	0.65 (0.50, 0.80)	< 0.001
	Venous	1.10 (1.00, 1.35)	1.00 (0.80, 1.30)	0.80 (0.63,	< 0.001

Notes: Normally distributed data are expressed as Mean ± SD, and non-normally distributed data as Median (P25, P75) (determined by Shapiro-Wilk normality test). Group comparisons were made using ANOVA or Kruskal-Wallis test, as appropriate.

Parameters	Phase	Adenocarcinoma (n = 81)	Squamous Cell Carcinoma (n = 38)	Small Cell Lung Cancer (n = 32)	*p*-value (Three-Group Comparison)
				1.00)	
	Delayed	1.20 (1.00, 1.40)	1.00 (0.80, 1.20)	0.80 (0.60, 1.00)	< 0.001
Normalized Iodine Concentration (NIC, %)	Arterial	9.72 ± 2.87	9.58 ± 3.39	7.12 ± 2.37	< 0.001
	Venous	32.90 (29.0, 37.2)	27.40 (20.1, 35.8)	26.10 (19.6, 29.4)	< 0.001
	Delayed	45.10 (40.5, 53.6)	41.45 (32.1, 47.5)	33.40 (27.8, 41.6)	< 0.001

Notes: Normally distributed data are expressed as Mean ± SD, and non-normally distributed data as Median (P25, P75) (determined by Shapiro-Wilk normality test). Group comparisons were made using ANOVA or Kruskal-Wallis test, as appropriate.

All triphasic DECT parameters showed significant differences (ICC 0.871 ~ 0.979, $p < 0.001$) with a consistent trend of AC > SCC > SCLC. SCLC had significantly lower CT40/80keV, λ_{HU}, IC, and NIC than AC/SCC in all phases. AC and SCC showed no arterial phase differences, but AC had higher venous/delayed phase IC/NIC and CT40/80keV than SCC. Delayed phase key parameters: AC IC 1.20 [1.05,1.35] mg/mL, SCC 1.00 [0.88,1.12] mg/mL, SCLC 0.80 [0.65,0.95] mg/mL; λ_{HU} AC 1.92 ± 0.42, SCC 1.64 ± 0.40, SCLC 1.25 ± 0.36.

Diagnostic Efficacy of Each Model

Univariate and multivariate Logistic regression analyses showed that the independent predictors for paired differentiation of different pathological types were different (Supplementary Table 3 and Table 3): AC vs. SCC (venous phase CT80keV, delayed phase IC, boundary, enhancement characteristics); AC vs. SCLC (arterial/delayed phase NIC, lesion diameter, pleural retraction); SCC vs. SCLC (delayed phase CT40keV, spiculation sign, lymph node fusion, enhancement characteristics).

Table 3
Multivariate Logistic Regression Independent Predictors for Subtype Differentiation

Subtype Pair	Independent Predictor	β	SE	*p*-value	OR (95% CI)
AC vs SCC	VP CT80keV	-0.207	0.105	0.048	0.813 (0.662–0.998)
	DP IC	0.006	0.002	0.001	1.006 (1.002–1.009)
	Margin (Ill-defined)	-1.302	0.543	0.016	0.272 (0.094–0.788)
	Enhancement (Markedly Hetero)	-1.713	0.531	0.001	0.180 (0.064–0.511)
AC vs SCLC	AP NIC (%)	0.556	0.239	0.02	1.745 (1.093–2.785)
	DP NIC (%)	0.237	0.084	0.005	1.268 (1.075–1.495)
	Diameter	-1.387	0.432	0.001	0.250 (0.107–0.582)
	Pleural Retraction (Present)	2.893	1.099	0.008	18.039 (2.094-155.368)
SCC vs SCLC	DP CT40keV	0.084	0.031	0.007	1.087 (1.023–1.155)
	Spiculation (Present)	3.932	1.209	0.001	51.031 (4.775-545.345)
	Mediastinal Lymph Node Fusion	-2.171	1.013	0.032	0.114 (0.016–0.830)
	Enhancement (Markedly Hetero)	1.747	0.76	0.022	5.740 (1.293–25.477)

Notes: All included variables were derived from dual-energy quantitative parameters (Iodine Concentration [IC], Normalized Iodine Concentration [NIC], CT value at 40 keV, CT value at 80 keV, spectral curve slope [λ_{HU}]) of triple-phase (arterial phase, venous phase, delayed phase) dual-source CT and CT Features with statistical differences (e.g., tumor location, enhancement heterogeneity); Abbreviations: AC, Adenocarcinoma, SCC, Squamous Cell Carcinoma, SCLC, Small Cell Lung Cancer; AP, arterial phase; DP, delayed phase; β, Regression Coefficient, SE, Standard Error, Z, Z-Statistic, *P, P*-Value, OR, Odds Ratio, 95%CI, 95% Confidence Interval.

Three diagnostic models were established, namely the DECT parameter model (constructed based on independent predictors of DECT parameters), the CT morphological model (constructed based on independent predictors of CT morphological features), and the combined model (integrating all identified independent predictors). The three models exhibited varying diagnostic performance in the pairwise differentiation of the three lung cancer pathological subtypes, with the combined model demonstrating the optimal overall efficacy (Table 4, Supplementary Table 4, and Fig. 3). Specifically, for AC vs. SCC, the

combined model achieved an AUC of 0.873 (95% CI: 0.809–0.936), with a sensitivity of 90.1% and a specificity of 71.1%; for AC vs. SCLC, the AUC was 0.980 (95% CI: 0.959–1.001), accompanied by a sensitivity of 95.1% and a specificity of 93.8%; and for SCC vs. SCLC, the AUC reached 0.937 (95% CI: 0.875–1.000), with a sensitivity of 89.5% and a specificity of 93.8%.

Table 4
Diagnostic Efficacy of Single and Combined Models

Subtype Pair	Model Type	AUC (95% CI)	Sensitivity (%)	Specificity (%)	Optimal Cutoff	*p*-value (vs Combined)
AC vs SCC	DECT Model	0.707 (0.604–0.810)	59.3	73.7	0.651	0.001
	Morphological Model	0.824 (0.745–0.903)	67.9	81.6	0.724	0.108
	Combined Model	0.873 (0.809–0.936)	90.1	71.1	0.546	-
AC vs SCLC	DECT Model	0.955 (0.920–0.990)	88.9	93.8	0.741	0.127
	Morphological Model	0.922 (0.863–0.981)	92.6	84.4	0.565	0.012
	Combined Model	0.980 (0.959–1.001)	95.1	93.8	0.588	-
SCC vs SCLC	DECT Model	0.859 (0.775–0.942)	68.4	87.5	0.597	0.06
	Morphological Model	0.853 (0.765–0.941)	78.9	81.3	0.475	0.02
	Combined Model	0.937 (0.875-1.000)	89.5	93.8	0.491	

Notes: Model definition: □DECT model: Constructed only based on triple-phase dual-energy quantitative parameters (IC, NIC, CT40keV, CT80keV, λ_{HU}) of dual-source CT; □Morphological Model: Constructed only based on Morphological Model with statistical differences (e.g., tumor location, margin, spiculation); □Combined model: Comprehensive diagnostic model integrating DECT Model and Morphological Model; Abbreviations: AUC, Area Under the Curve, CI, Confidence Interval; AC, Adenocarcinoma, SCC, Squamous Cell Carcinoma, SCLC, Small Cell Lung Cancer.

Discussion

This study enrolled three clinically core types of lung cancer (AC, SCC, and SCLC; typical images see Fig. 4) and comprehensively analyzed the triphasic DECT parameters (arterial, venous, and delayed phases). It was found that the delayed phase parameters (such as delayed phase IC, NIC, CT40keV/80keV, and λ_{HU}) showed stable type-specific gradient differences (AC > SCC > SCLC), with statistically significant differences between each pair of the three groups. This fills the research gap in the application of delayed phase DECT quantitative parameters in the differentiation of the three lung cancer types (AC, SCC, and SCLC). Meanwhile, the specific independent predictors for paired differentiation of different types were identified (e.g., differentiation between AC and SCC relies on venous phase CT80keV and delayed phase IC; differentiation between AC and SCLC requires the combination of arterial/delayed phase NIC and pleural retraction sign; delayed phase CT40keV and spiculation sign are key for differentiating SCC and SCLC), making the differentiation approach more targeted. Furthermore, a combined model of DECT parameters and CT morphological features was constructed, which achieved an AUC of up to 0.980 (sensitivity: 95.1%, specificity: 93.8%) in differentiating AC from SCLC and an AUC of 0.937 in differentiating SCC from SCLC, significantly outperforming the single CT morphological model or DECT model. Additionally, the integrated CT morphological features (such as boundary, enhancement characteristics, and mediastinal lymph node fusion) are all easily accessible indicators in routine clinical imaging evaluation. This model not only retains the quantitative advantages of DECT parameters but also takes into account clinical practicality, providing a more accurate and operable typing scheme for scenarios lacking pathological biopsy conditions (e.g., deeply located tumors, poor patient tolerance).

The results of this study compared the qualitative and quantitative parameters of three pathological types of lung cancer (AC, SCC, and SCLC). Previous DECT studies have mostly been limited to differentiating two pathological subtypes (5, 6, 16, 17). In contrast, this study is the first to cover three core subtypes simultaneously, completing paired differentiation for AC-SCC, AC-SCLC, and SCC-SCLC. This fills the gap in evidence regarding the simultaneous differentiation of the three subtypes and better aligns with clinical demands for multi-subtype differentiation. In terms of scanning phases, this study added the delayed phase to the conventional arterial and venous phases, confirming that delayed phase parameters—including iodine concentration (IC), normalized iodine concentration (NIC), and CT40keV values—exhibit significant differences among the three groups and serve as independent predictors for certain paired differentiations. These findings indicate that delayed phase parameters can capture the dynamic characteristics of tumor blood supply and metabolism, thereby improving diagnostic efficacy. For model construction, this study optimized predictors separately for each of the three paired differentiations, and the constructed combined model of DECT parameters and CT morphological features achieved superior diagnostic efficacy compared with most previous models for single paired differentiation. Meanwhile, a systematic analysis of 13 CT morphological features identified that features such as mediastinal lymph node fusion and vascular involvement have specific diagnostic value for SCLC, further enriching the clinical evidence system for differentiating lung cancer pathological subtypes using DECT (18). From a pathological mechanism perspective, the differences in DECT quantitative parameters are directly associated with the histological characteristics of tumors: AC is

dominated by glandular tubular structures with abundant blood supply; SCC typically exhibits solid nest-like growth and is prone to necrosis; SCLC is a highly aggressive neuroendocrine tumor characterized by extensive necrosis and poor vascularization (3, 19). In this study, the triphasic values of CT40keV, CT80keV, λ_{HU}, IC, and NIC in SCLC were significantly lower than those in AC and SCC. This is consistent with the pathological features of SCLC, where extensive necrosis reduces iodine uptake, whereas NSCLC subtypes have richer vascular. These results corroborate the correlation between DECT parameters (IC and NIC) and tumor vascularization degree as well as necrosis status (6, 17). The parameter differences between AC and SCC were more pronounced in the venous and delayed phases, which aligns with the traits of AC (higher micro-vessel density) and SCC (restricted contrast agent penetration and delayed blood supply, leading to lower iodine accumulation in the venous phase) (4, 20). Notably, delayed phase parameters emerged as key factors for pairwise differentiation of the three lung cancer subtypes, addressing the limitation of existing studies that only applied delayed phase parameters for differentiating benign and malignant pulmonary lesions rather than conducting in-depth subtype comparisons (14). By reflecting contrast agent retention characteristics, delayed phase information provides a supplementary perspective beyond the venous phase for lung cancer subtyping, amplifying vascular-stromal differences among subtypes and offering important reference values for cases with inconclusive venous phase differentiation (11, 21). In this study, NIC demonstrated slightly better diagnostic efficacy than IC, possibly because NIC minimizes interference from factors such as patient circulation status and contrast agent injection (9, 17). However, the diagnostic performance for differentiating AC and SCC was relatively limited, which may be attributed to the fact that both belong to NSCLC, sharing overlapping histopathological features and blood supply patterns, with parameter crossover induced by tumor heterogeneity (4, 9).

This study has the following limitations: First, this study adopted a single-center prospective design, with a relatively limited sample size of 151 cases, and no multi-center external validation was performed. Compared with some large-sample studies, the generality and robustness of the results need to be further verified, and there may be selection bias; second, the study did not include potential confounding factors such as tumor differentiation degree and gene mutation status (e.g., EGFR mutation), while previous studies have shown that pathological grade (22) and driver gene mutation (10) may affect DECT quantitative parameters (e.g., iodine concentration, spectral curve slope), which may interfere with diagnostic efficacy; third, the ROI of quantitative parameters relies on manual delineation by radiologists, which may cause selection bias; finally, this study only explored the directly measured parameters of DECT. In the future, further exploration of DECT-derived parameters (e.g., extracellular volume, enhancement ratio in different phases (14, 23, 24) and radiomics modeling (18, 22) can be conducted to further improve the accuracy of differentiation.

In conclusion, the predictive model combining dual-source CT dual-energy quantitative parameters (including arterial, venous, and delayed phases) with CT morphological features has the optimal efficacy in differentiating the three core types of lung cancer (adenocarcinoma, squamous cell carcinoma, small cell lung cancer), especially the highest accuracy in differentiating adenocarcinoma from small cell lung cancer; delayed phase quantitative parameters provide key supplements for type differentiation, filling

the gap in previous studies, and can provide a non-invasive and accurate typing basis for clinical practice.

Abbreviations

AC
Adenocarcinoma
AP
Arterial Phase
AUC
Area Under the Curve
CI
Confidence Interval
CT
Computed Tomography
DECT
Dual-energy Computed Tomography
DLP
Dose-Length Product
DP
Delayed Phase
HU
Hounsfield Unit
ICC
Intraclass Correlation Coefficient
IC
Iodine Concentration
λ_{HU}
Spectral Curve Slope
NIC
Normalized Iodine Concentration
NSCLC
Non-small Cell Lung Cancer
ROI
Region of Interest
ROC
Receiver Operating Characteristic
SCC
Squamous Cell Carcinoma
SCLC

Small Cell Lung Cancer
TNM
Tumor-Node-Metastasis
VMI
Virtual Monoenergetic Image
VP
Venous Phase

Declarations

Ethics approval and consent to participate

This study was approved by the Ethics Committee of our hospital (approval number: GYLLPJ-2022049), and all patients signed informed consent forms prior to the examination.

Consent for publication

Not applicable.

Competing interests

Two authors of this manuscript, Li'an Luo and Lveqin Huang, are employees of Siemens Healthineers, but they were not involved in the acquisition of the data and had no control of data or information submitted for publication. There is no conflict of interest or industry support in this study. All other authors declare no competing interests.

Clinical trial number

Not applicable.

Funding

Not applicable.

Author Contribution

(I) Conception and design: Dongmei Liang and Hanhuan Liang(II) Administrative support: Hanhuan Liang(III) Provision of study materials or patients: Hong Zhang,Hongyan Ren, Yayi Zou and Shitao Huang(IV) Collection and assembly of data: Dongmei Liang, Hong Zhang and Keyu Peng(V) Data

analysis and interpretation: Dongmei Liang, Li’an Luo and Lveqin Huang(VI) Manuscript writing: All authors(VII) Final approval of manuscript: All authors

Acknowledgements

Not applicable.

Availability of data and materials

The data that support the findings of this study are available from the corresponding author upon reasonable request. The data is not publicly available due to privacy and ethical restrictions of the hospital.

References

1. Bray F, Laversanne M, Sung H, Ferlay J, Siegel RL, Soerjomataram I, et al. Global cancer statistics 2022: GLOBOCAN estimates of incidence and mortality worldwide for 36 cancers in 185 countries. CA Cancer J Clin. 2024;74(3):229–63. 10.3322/caac.21834.
2. Ferrari AJ, Santomauro DF, Aali A, Abate YH, Abbafati C, Abbastabar H, et al. Global incidence, prevalence, years lived with disability (YLDs), disability-adjusted life-years (DALYs), and healthy life expectancy (HALE) for 371 diseases and injuries in 204 countries and territories and 811 subnational locations, 1990–2021: a systematic analysis for the Global Burden of Disease Study 2021. Lancet. 2024;403(10440):2133–61. 10.1016/S0140-6736(24)00757-8.
3. García-Campelo R, Sullivan I, Arriola E, Insa A, Juan Vidal O, Cruz-Castellanos P, et al. SEOM-GECP Clinical guidelines for diagnosis, treatment and follow-up of small-cell lung cancer (SCLC) (2022). Clin Transl Oncol. 2023;25(9):2679–91. 10.1007/s12094-023-03216-3.
4. Zhang Z, Zou H, Yuan A, Jiang F, Zhao B, Liu Y, et al. A Single Enhanced Dual-Energy CT Scan May Distinguish Lung Squamous Cell Carcinoma From Adenocarcinoma During the Venous phase. Acad Radiol. 2020;27(5):624–9. 10.1016/j.acra.2019.07.018.
5. Mu R, Meng Z, Guo Z, Qin X, Huang G, Yang X, et al. Diagnostic value of dual-layer spectral detector CT in differentiating lung adenocarcinoma from squamous cell carcinoma. Front Oncol. 2022;12:868216. 10.3389/fonc.2022.868216.
6. Xu X, Sui X, Zhong W, Xu Y, Wang Z, Jiang J, et al. Clinical utility of quantitative dual-energy CT iodine maps and CT morphological features in distinguishing small-cell from non-small-cell lung cancer. Clin Radiol. 2019;74(4):268–77. 10.1016/j.crad.2018.10.012.
7. Kim C, Kim W, Park SJ, Lee YH, Hwang SH, Yong HS, et al. Application of Dual-Energy Spectral Computed Tomography to Thoracic Oncology Imaging. Korean J Radiol. 2020;21(7):838. 10.3348/kjr.2019.0711.

8. Hartley-Blossom ZJ, Digumarthy SR. Dual-Energy Computed Tomography Applications in Lung Cancer. Radiol Clin North Am. 2023;61(6):987–94. 10.1016/j.rcl.2023.06.001.
9. Ma X, Xu M, Tian XJ, Liu YL, Zhang XR, Qiao Y. A Retrospectively Study: Diagnosis of Pathological Types of Malignant Lung Tumors by Dual-layer Detector Spectral Computed Tomography. Technol Cancer Res Treat. 2022;21:15330338221074498. 10.1177/15330338221074498.
10. Li F, Qi L, Cheng S, Liu J, Chen J, Cui S, et al. Predicting epidermal growth factor receptor mutations in non-small cell lung cancer through dual-layer spectral CT: a prospective study. Insights Imaging. 2024;15(1):109. 10.1186/s13244-024-01678-9.
11. Chen Y, Jiang J, Yan C, Jiang J, Shi B, Xu Z, et al. Prediction of tumor regression grade in far-advanced gastric cancer after preoperative immuno-chemotherapy using dual-energy CT-derived extracellular volume fraction. Eur Radiol. 2024;35(1):93–104. 10.1007/s00330-024-10737-0.
12. Deng L, Yang J, Zhang M, Zhu K, Zhang J, Ren W, et al. Predicting lymphovascular invasion in N0 stage non-small cell lung cancer: A nomogram based on Dual–energy CT imaging and clinical findings. Eur J Radiol. 2024;179:111650. 10.1016/j.ejrad.2024.111650.
13. Li Q, Li X, Li XY, Huo JW, Lv FJ, Luo TY. Spectral CT in Lung Cancer: Usefulness of Iodine Concentration for Evaluation of Tumor Angiogenesis and Prognosis. Am J Roentgenol. 2020;215(3):595–602. 10.2214/AJR.19.22688.
14. Jiang X, Ma Q, Zhou T, Feng Q, Yang W, Zhou X, et al. Extracellular volume fraction as a potential predictor to differentiate lung cancer from benign lung lesions with dual-layer detector spectral CT. Quant Imaging Med Surg. 2023;13(12):8121–31. 10.21037/qims-23-736.
15. Kastner J, Hossain R, Jeudy J, Dako F, Mehta V, Dalal S, et al. Lung-RADS Version 1.0 versus Lung-RADS Version 1.1: Comparison of Categories Using Nodules from the National Lung Screening Trial. Radiology. 2021;300(1):199–206. 10.1148/radiol.2021203704.
16. Zheng X, Tian H, Li W, Li J, Xu K, Jin C, et al. The diagnosis value of dual-energy computed tomography (DECT) multi-parameter imaging in lung adenocarcinoma and squamous cell carcinoma. BMC Pulm Med. 2024;24(1):545. 10.1186/s12890-024-03370-6.
17. Mu R, Meng Z, Zhang X, Guo Z, Zheng W, Zhuang Z, et al. Parameters of Dual-layer Spectral Detector CT Could be Used to DifferentiateNon-Small Cell Lung Cancer from Small Cell Lung Cancer. CMIR. 2022;18(10):1070–8. 10.2174/1573405618666220308105359.
18. Lin Z, Liu Y, Xia C, Huang P, Peng Z, Yi L, et al. Dual-energy CT Radiomics Combined with Quantitative Parameters for Differentiating Lung Adenocarcinoma From Squamous Cell Carcinoma: A Dual-center Study. Acad Radiol. 2025;32(3):1675–84. 10.1016/j.acra.2024.09.024.
19. Zheng M, Classification, Pathology of Lung Cancer. Surg Oncol Clin N Am. 2016;25(3):447–68. 10.1016/j.soc.2016.02.003.
20. Cheng Z, Wang Y, Yuan M, Liang J, Feng Y, Shi Y, et al. CT perfusion imaging can detect residual lung tumor early after radiofrequency ablation: a preliminary animal study on both tumoral and peri-tumoral region assessment. J Thorac Dis. 2022;14(1):64–75. 10.21037/jtd-21-967.

21. Luo Y, Liu L, Liu D, Shen H, Wang X, Fan C, et al. Extracellular volume fraction determined by equilibrium contrast-enhanced CT for the prediction of the pathological complete response to neoadjuvant chemoradiotherapy for locally advanced rectal cancer. Eur Radiol. 2022;33(6):4042–51. 10.1007/s00330-022-09307-z.
22. Zheng Y, Li H, Zhang K, Luo Q, Ding C, Han X, et al. Dual-energy CT-based radiomics for predicting pathological grading of invasive lung adenocarcinoma. Clin Radiol. 2024;79(10):e1226–34. 10.1016/j.crad.2024.07.009.
23. Xie X, Liu K, Luo K, Xu Y, Zhang L, Wang M, et al. Value of dual-layer spectral detector computed tomography in the diagnosis of benign/malignant solid solitary pulmonary nodules and establishment of a prediction model. Front Oncol. 2023;13:1147479. 10.3389/fonc.2023.1147479.
24. Liu K, Wang M, Xu Y, Chen Q, Li K, Zhang L, et al. Value of spectral computed tomography-derived quantitative parameters based on full volume analysis in the diagnosis of benign/malignant and pathological subtypes of solitary pulmonary nodules. Quant Imaging Med Surg. 2023;13(6):3827–40. 10.21037/qims-22-979.

Figures

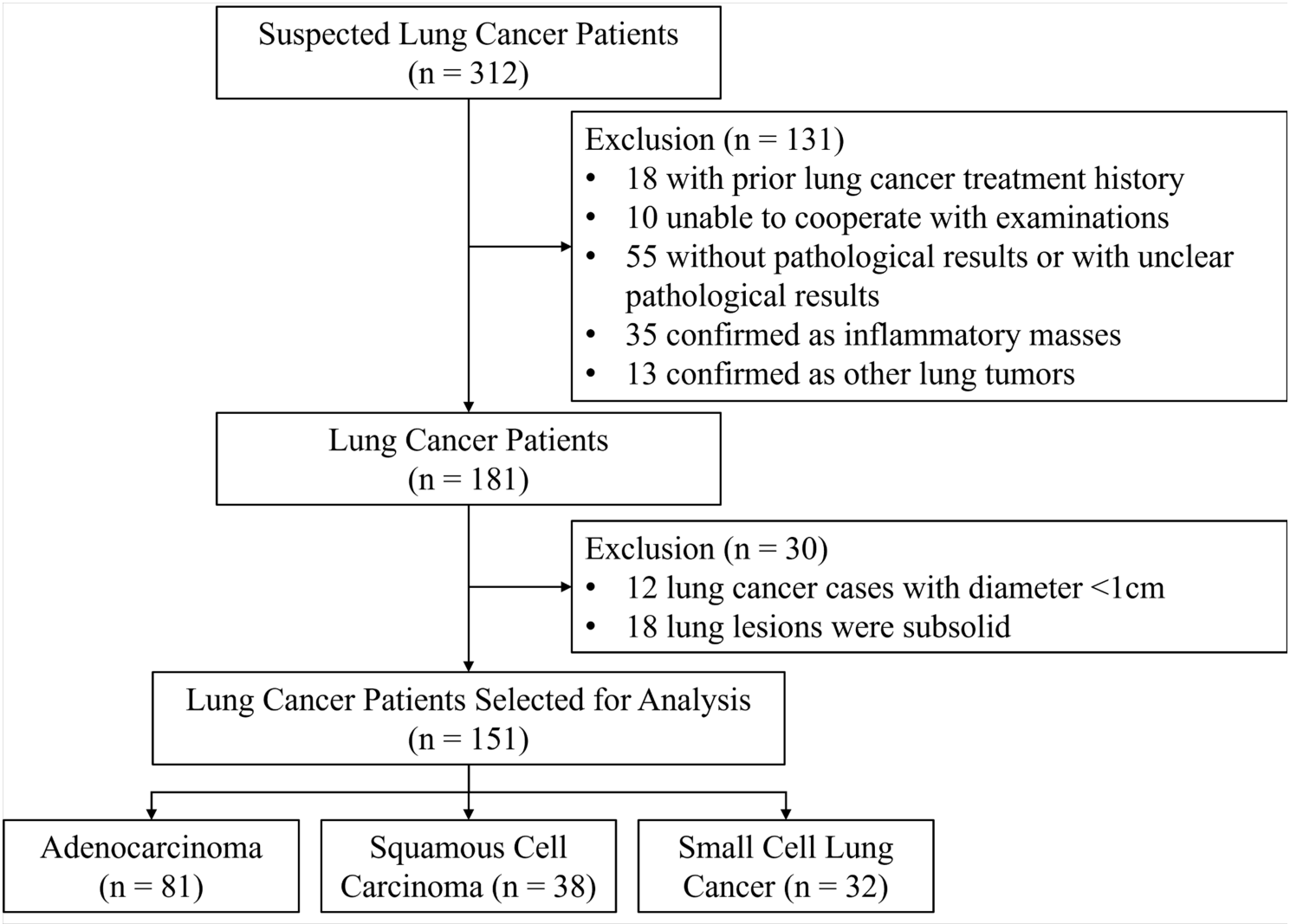


Figure 1

Study flowchart

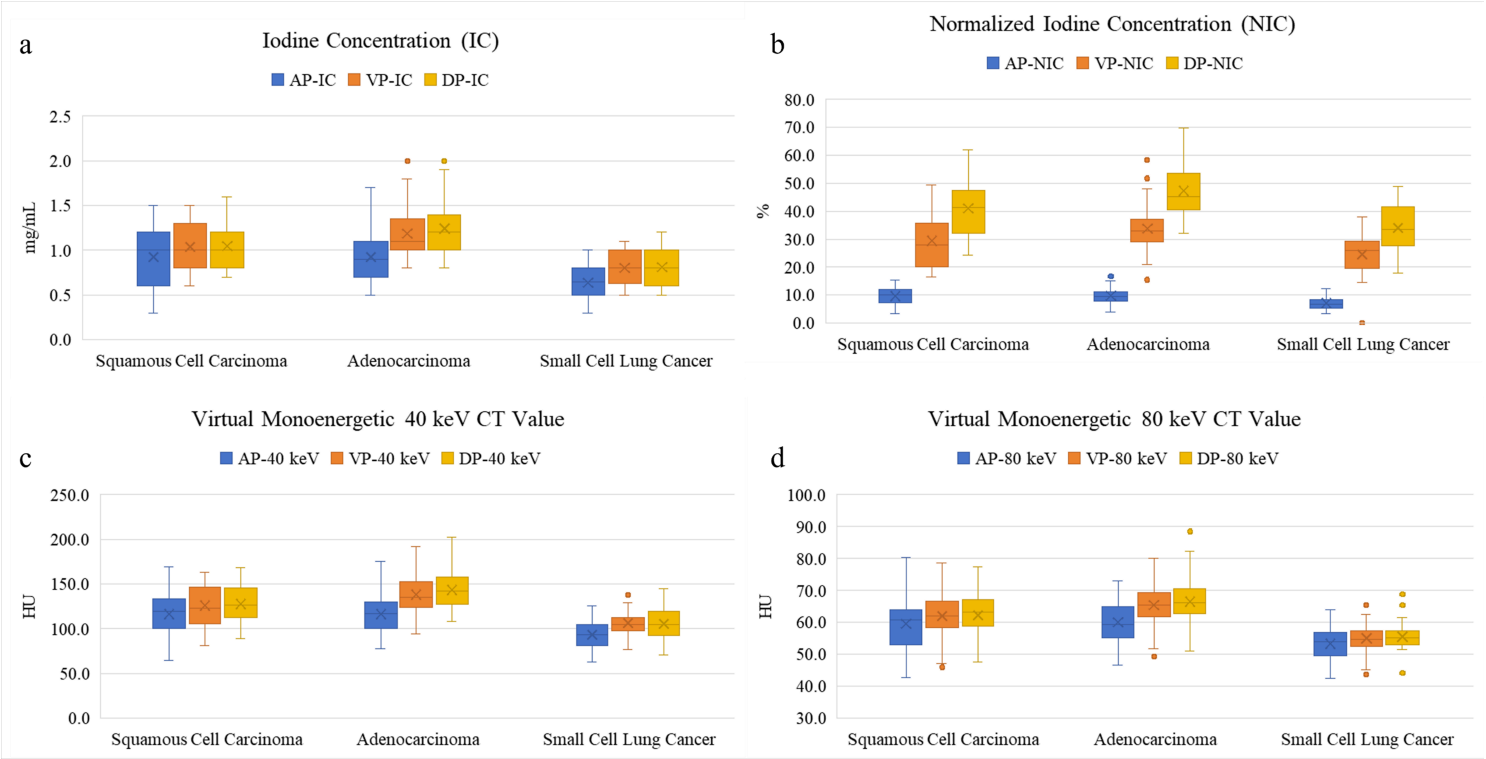


Figure 2

DECT quantitative parameters of different lung cancer subtypes across three enhancement phases. AP, Arterial Phase, VP, Venous Phase, DP, Delayed Phase; IC, Iodine Concentration, NIC, Normalized Iodine Concentration; SCC, Squamous Cell Carcinoma, AC, Adenocarcinoma, SCLC, Small Cell Lung Cancer; HU, Hounsfield Unit.

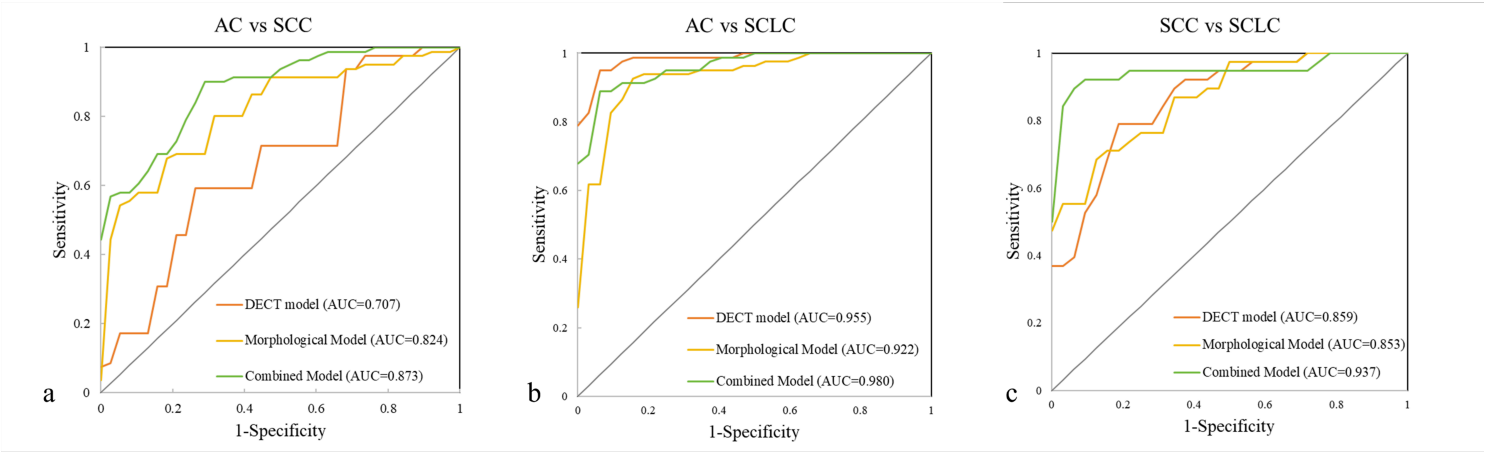


Figure 3

Receiver operating characteristic (ROC) curves of different models for differentiating lung cancer subtypes. The DECT model refers to the dual-energy CT parameter model, the Morphological Model refers to the CT sign model, and the Combined Model refers to the integrated model of dual-energy CT parameters and CT signs. AC, adenocarcinoma, SCC, squamous cell carcinoma, SCLC, small cell lung cancer; AUC, Area Under the Curve.

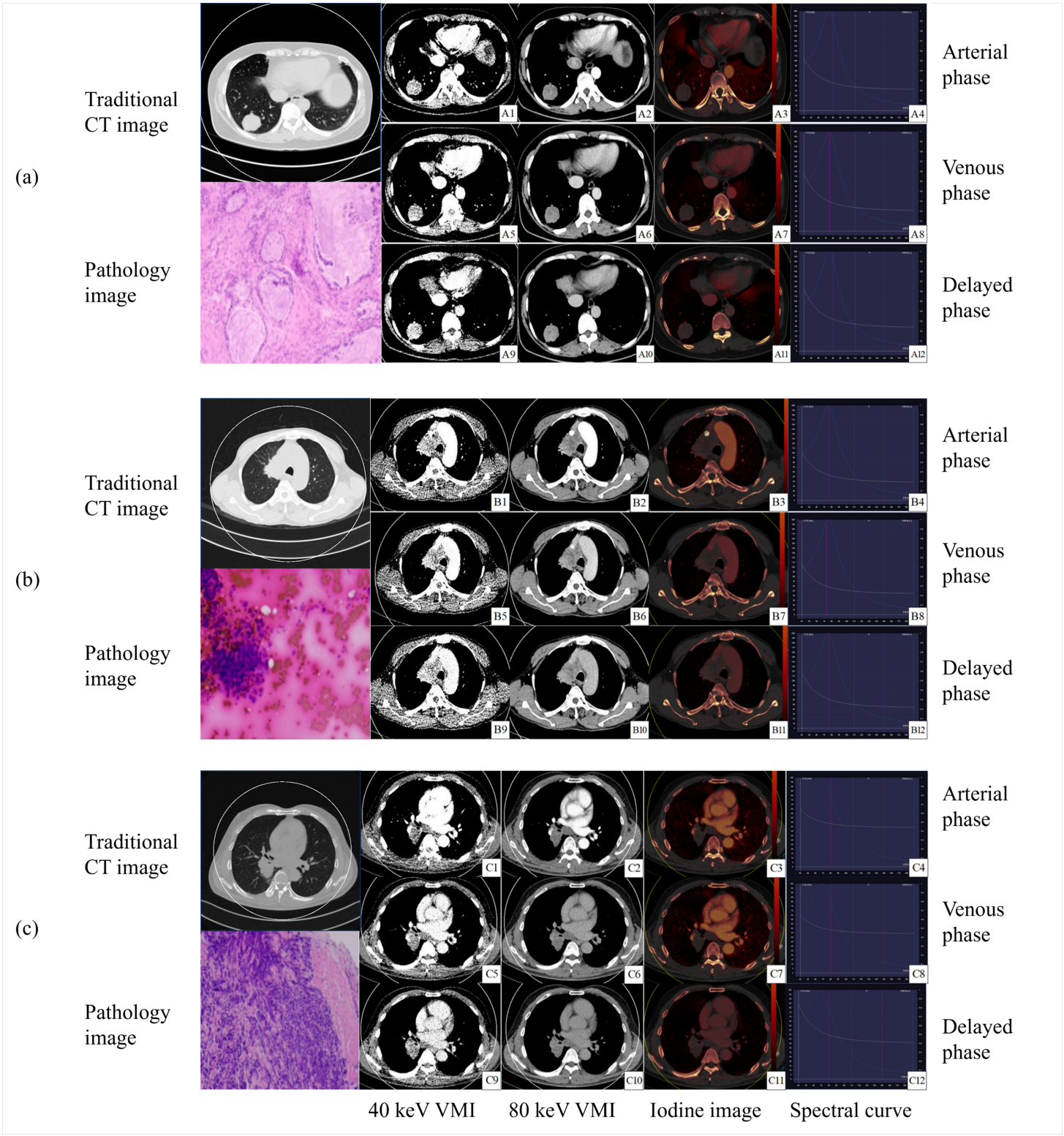


Figure 4

Representative pathology and DECT images of three types of lung lesions. (a) A 45-year-old female with right lower lobe peripheral mass was diagnosed with invasive mucinous adenocarcinoma. Immunohistochemistry: CK8 (+), TTF-1 (+), NapsinA (+). DECT: Arterial phase: 40 keV 112.5 HU, 80 keV 56.2 HU, IC 1.0 mg/mL, NIC 10.1%; Venous phase: 40 keV 120.2 HU, 80 keV 56.6 HU, IC 1.0 mg/mL, NIC 35.6%; Delayed phase: 40 keV 134.1 HU, 80 keV 60.3 HU, IC 1.2 mg/mL, NIC 58.4%. Delayed IC/NIC elevation + peripheral morphology supports diagnosis. (b) A 78-year-old male with right upper lobe paramediastinal mass was diagnosed with poorly differentiated squamous cell carcinoma. Immunohistochemistry: P40 (focal +), P63 (+), CK5 (focal +). DECT: Arterial phase: 40 keV 112.0 HU, 80 keV 54.1 HU, IC 0.9 mg/mL, NIC 10.1%; Venous phase: 40 keV 113.4 HU, 80 keV 59.5 HU, IC 0.9 mg/mL, NIC 22.6%; Delayed phase: 40 keV 119.1 HU, 80 keV 60.4 HU, IC 1.0 mg/mL, NIC 34.1%. Enhancement heterogeneity + quantitative features + central morphology aids pathological typing. (c) A 60-year-old male with right lower lobe hilar-adjacent mass was diagnosed with small cell lung cancer (SCLC). Immunohistochemistry: CD56 (focal +), CgA (+), SYN (+), Ki-67 (100% + in hot spots). DECT: Arterial phase: 40 keV 92.5 HU, 80 keV 52.3 HU, IC 0.7 mg/mL, NIC 7.0%; Venous phase: 40 keV 112.8 HU, 80 keV 56.8 HU, IC 0.8 mg/mL, NIC 27.0%; Delayed phase: 40 keV 124.3 HU, 80 keV 58.4 HU, IC 1.0 mg/mL, NIC 38.5%. Low arterial IC + progressive enhancement + central mass/mediastinal lymph node fusion provides quantitative evidence for this aggressive subtype. DECT, Dual-energy CT; NIC, normalized iodine concentration; VMI, Virtual Monoenergetic image.

Supplementary Files

This is a list of supplementary files associated with this preprint. Click to download.

- SupplementaryTable1.docx
- SupplementaryTable2.docx
- SupplementaryTable3.docx
- SupplementaryTable4.docx
- supplementarymaterialSTARD2015Checklist.docx
- supplementarymaterialcoidisclosure.docx